Supplementary Information to : Emergence of tunable periodic density correlations in a Floquet-Bloch system

N. Dupont[1], L. Gabardos[1], F. Arrouas[1], G. Chatelain[1], M. Arnal[1], J. Billy[1], P. Schlagheck[2], B. Peaudecerf[1], D. Guéry-Odelin[1]*

[1] *Laboratoire Collisions Agrégats Réactivité, UMR 5589, FERMI, UT3, Université de Toulouse, CNRS, 118 Route de Narbonne, 31062 Toulouse CEDEX 09, France*

[2] *CESAM Research Unit, University of Liège, 4000 Liège, Belgium*

1. Production of BECs

In our experiment, approximately $2 \cdot 10^9$ atoms from a 3D magneto-optical trap are initially loaded into a magnetic quadrupole. The quadrupole gradient is then ramped up to 1.8 T/m to allow for microwave evaporation. After evaporation over 10 s the temperature of the atom cloud is decreased from 300 μK to 30 μK. Subsequently, while keeping a small magnetic gradient for gravity compensation, the atoms are transferred to a crossed dipole trap [1], made of two 1064 nm laser beams, with waist 45 μm and maximum power 4 W, crossing in the horizontal plane with a 16° angle. The evaporation in this final dipole trap yields a pure BEC of up to $5 \cdot 10^5$ atoms in the low-field-seeker state $|F = 1, m_F = -1\rangle$. The lattice beams are aligned on one of the dipole trap beams, leading to an 8° angle between the lattice axis Ox and the principal axis Ox' of the hybrid trap (crossed dipole trap + magnetic quadrupole) in which the BEC is obtained. The hybrid trap is characterized by the angular frequencies $(\omega_{x'}, \omega_{y'}, \omega_z) = 2\pi \times (10.4, 66, 68)$ Hz, where the horizontal axis Oy' is orthogonal to Ox', and Oz is the vertical axis.

2. Tight-binding effective model

a. *Model and instability*

We model the resonant coupling between bands at $q \neq 0$ in the modulated lattice by an effective tight-binding model with two coupled bands that reproduces the main features of a typical Floquet spectrum, described by the effective Hamiltonian :

$$\begin{aligned}
\hat{H}_{\text{eff}} =& \hat{H}_0 + \hat{H}_{\text{int}} \\
\hat{H}_0 =& -J_0 \sum_\ell \hat{a}^\dagger_{\ell+1}\hat{a}_\ell + \hat{a}^\dagger_\ell \hat{a}_{\ell+1} - J_1 \sum_\ell \hat{b}^\dagger_{\ell+1}\hat{b}_\ell + \hat{b}^\dagger_\ell \hat{b}_{\ell+1} \\
&+ E_b \sum_\ell \hat{b}^\dagger_\ell \hat{b}_\ell + W \sum_\ell \hat{b}^\dagger_\ell \hat{a}_\ell + \hat{a}^\dagger_\ell \hat{b}_\ell \\
\hat{H}_{\text{int}} =& \frac{U}{2} \sum_\ell \hat{a}^{\dagger 2}_\ell \hat{a}^2_\ell,
\end{aligned} \tag{1}$$

where $\hat{a}_\ell$ (resp. $\hat{b}_\ell$) are the annihilation operators for band 0 (resp. 1) on site ℓ of the one-dimensional lattice, $J_{0,1}$ are the tunneling amplitudes for the two bands ($J_0 > 0$ and $|J_0| < |J_1|$), E_b is an energy offset for band 1, W is a coupling amplitude, and U is an effective on-site interaction energy (see SI Appendix 3).

The condensate is considered initially in the ground mode of band 0 with $\langle \hat{a}_\ell \rangle = \sqrt{n}$, and associated chemical potential $\mu = -2J_0 + nU$. We then study the stability of this initial condensate due to the interaction term, through a perturbative Bogolubov treatment. The coupled-band Hamiltonian $\hat{H}_0$ describes two hybridized energy bands u and v with energies $E_{u,v}(q)$, as a function of quasi-momentum q:

$$\begin{aligned}
E_u(q) &= \left[E_0(q) \cos^2\left(\frac{\theta}{2}\right) + E_1(q) \sin^2\left(\frac{\theta}{2}\right) \right] + W \sin(\theta), \\
E_v(q) &= \left[E_0(q) \sin^2\left(\frac{\theta}{2}\right) + E_1(q) \cos^2\left(\frac{\theta}{2}\right) \right] - W \sin(\theta).
\end{aligned}$$

where $E_0(q) = -2J_0 \cos(q)$ and $E_1(q) = -2J_1 \cos(q) + E_b$ are the energies of the uncoupled bands, and $\theta(q)$ is the mixing angle defined by:

$$\tan(\theta(q)) = \frac{2W}{(E_0(q) - E_1(q))}, \; 0 \leq \theta < \pi.$$

We write the fields orthogonal to the condensate mode as :

* dgo@irsamc.ups-tlse.fr

$$\delta\hat{\psi}^{\perp}_{a,\ell} = \int_{-\pi}^{\pi} \frac{e^{iq\ell}}{\sqrt{2\pi}} \hat{\Lambda}_{0,q}\, \mathrm{d}q$$
$$\delta\hat{\psi}^{\perp}_{b,\ell} = \int_{-\pi}^{\pi} \frac{e^{iq\ell}}{\sqrt{2\pi}} \hat{\Lambda}_{1,q}\, \mathrm{d}q$$

where we have introduced the number conserving operators $\hat{\Lambda}_{0,q}$ (resp. $\hat{\Lambda}_{1,q}$) which describe the transfer of an atom from the mode at momentum q of band 0 (resp. band 1) to the condensate mode [2].

The quadratic part of the expansion of $\hat{H}_{\text{eff}}$ in the fields $\hat{\Lambda}$ yields a set of linearized evolution equations, which can be summarized as

$$i\hbar \frac{\mathrm{d}}{\mathrm{d}t} \begin{pmatrix} \hat{\Lambda}_{0,q} \\ \hat{\Lambda}_{1,q} \\ \hat{\Lambda}^{\dagger}_{0,-q} \\ \hat{\Lambda}^{\dagger}_{1,-q} \end{pmatrix} = \mathcal{L}_q \begin{pmatrix} \hat{\Lambda}_{0,q} \\ \hat{\Lambda}_{1,q} \\ \hat{\Lambda}^{\dagger}_{0,-q} \\ \hat{\Lambda}^{\dagger}_{1,-q} \end{pmatrix} \tag{2}$$

where $\mathcal{L}_q$ is block matrix made of the 2-by-2 matrices $\hat{A}_q$ and $\hat{B}_q$, with definitions:

$$\mathcal{L}_q = \begin{pmatrix} \hat{A}_q & \hat{B}_q \\ -\hat{B}_q & -\hat{A}_q \end{pmatrix}$$
$$\hat{A}_q = \begin{pmatrix} E_0(q) - \mu + 2nU & W \\ W & E_1(q) - \mu \end{pmatrix}$$
$$\hat{B}_q = \begin{pmatrix} nU & 0 \\ 0 & 0 \end{pmatrix}$$

The modes at q are stable if the eigenvalues of the matrix $\mathcal{L}_q$ are all real. In practice we may search for the largest imaginary part among all eigenvalues to characterize instability.

Illustration. We illustrate the model with conditions similar to those of Fig. 1at a frequency $\nu = 30\,\mathrm{kHz}$. We have represented the Floquet spectrum of the modulated lattice (Fig. S1**(a)**), and the model spectrum (Fig. S1**(b)**) of Hamiltonian $\hat{H}_0$ (see equation 1), with parameters adjusted so that the coupled bands best reproduce the avoided crossings between the s and d bands in the Floquet system (in units of E_L, $J_0 = 0.0021$, $J_1 = -0.2796$, $E_b = 0.2593$ and $W = 0.051$). In Fig. S1**(c)** we plot the instability exponent defined as the absolute value of the largest imaginary part among the four eigenvalues, for a varying value of the interaction parameter nU (see Section 3). Two narrow regions of q in the vicinity of the avoided crossings lead to pure imaginary eigenvalues, with maximally unstable modes.

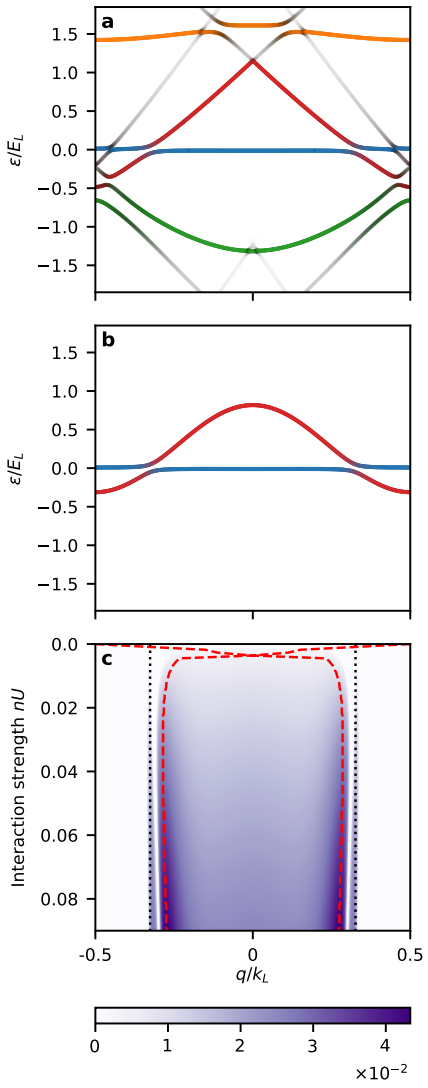

FIG. S1. **Tight-binding model of the instability. (a)** Floquet spectrum of the modulated system for parameters $s_0 = 3.4$, $\nu = 30\,\mathrm{kHz}$ and $\varphi_0 = 20°$. Overlap with the states of the static lattice bands is color-coded with blue, orange, green and red corresponding respectively to the first 4 bands (s to f). **(b)** Spectrum of the model Hamiltonian H_0 (see equation 1) with two coupled, tightly-bound bands. Adjusted parameters (see text) are (in units of E_L) $J_0 = 0.0021$, $J_1 = -0.2796$, $E_b = 0.2593$ and $W = 0.051$ (a global offset is applied to match the Floquet spectrum in (a)). **(c,d)** Maximum instability exponent of the Bogolubov matrix (2), as a function of quasi-momentum and the interaction parameter nU. The position of the band crossing and the maximum exponent over the Brillouin zone are plotted in dotted black and dashed red lines respectively.

b. *Onset of correlations from the instability*

Based on the previous mode decomposition, we can write a general expression for the elements of the reduced one-body density matrix :

$$\langle \hat{a}^{\dagger}_l(t)\hat{a}_{l'}(t)\rangle = n + \int_{-\pi}^{\pi} \frac{e^{iq(l'-l)}}{2\pi} \langle \hat{\Lambda}^{\dagger}_{0,q}(t)\hat{\Lambda}_{0,q}(t)\rangle\, \mathrm{d}q \tag{3}$$

Due to the symmetries of the Bogolubov matrix $\mathcal{L}_q$, and near the maximum of the instability exponent, its eigenvalues come in pairs of opposite real and imaginary values, which we denote $\{\omega_q, -\omega_q, i\lambda_q, -i\lambda_q\}$ with the convention $\omega_q, \lambda_q > 0$. Using the fact that none of the modes with $q \neq 0$ is initially populated, the expression of the average value in Equation (3) can be obtained and is approximately equal to:

$$\langle \hat{\Lambda}^\dagger_{0,q}(t)\hat{\Lambda}_{0,q}(t)\rangle \simeq |u_q|^2(1+|v_q|^2)e^{2\lambda_q t} \tag{4}$$

keeping the exponentially diverging terms only, where the coefficients u_q, v_q are the coefficients of the eigenvector of $\mathcal{L}_q$ for the eigenvalue $i\lambda_q$, which is generally of the form $(u_q, v_q, iu_q^*, iv_q^*)^T$.

Let us now consider the vicinity of a maximum of the instability exponent λ_q, near some $q = q^* > 0$. We have

$$\lambda_q \simeq \lambda_* - \frac{\lambda''}{2}(q-q^*)^2 + O\left((q-q^*)^3\right) \tag{5}$$

with $\lambda_* > 0$. Due to the symmetry of the band structure, the same behavior arises near $q = -q^*$,

$$\lambda_q \simeq \lambda_* - \frac{\lambda''}{2}(q+q^*)^2 + O\left((q+q^*)^3\right) \tag{6}$$

We can then evaluate Eq. (3) with the saddle-point approximation. This yields the estimate

$$\langle \hat{a}^\dagger_l(t)\hat{a}_{l'}(t)\rangle \simeq n + 2n^*(t)e^{-(l-l')^2/\Delta^2(t)}\cos[(l-l')q^*] \tag{7}$$

with

$$\Delta(t) = 2\sqrt{\lambda'' t}\,, \tag{8}$$

with the time-dependent population

$$n^*(t) = \frac{|u_{q^*}|^2(1+|v_{q^*}|^2)}{\sqrt{\pi}\Delta(t)}e^{2\lambda_* t} \tag{9}$$

of excitations near the modes of momentum q^*. This implicitly assumes that this population stays much smaller than the remaining condensate population n at all times.

A very similar result is obtained for the density-density correlation function. Defining the site population operator $\hat{n}_l = \hat{a}^\dagger_l\hat{a}_l$ and the mean site occupancy $\bar{n} = \langle \hat{n}_l\rangle = n + 2n^*$, and using $n^*(t) \ll n$, we obtain, to first order in n^*

$$\begin{aligned} g^{(2)}(l-l') - 1 &= \frac{\langle \hat{n}_l(t)\hat{n}_{l'}(t)\rangle}{\langle \hat{n}_l(t)\rangle\langle \hat{n}_{l'}(t)\rangle} - 1 \\ &\simeq 4\frac{nn^*(t)}{\bar{n}^2}e^{-(l-l')^2/\Delta^2(t)}\cos[(l-l')q^*] - \frac{\delta_{ll'}}{\bar{n}}\,. \end{aligned} \tag{10}$$

We therefore have a normalized coherence $g^{(1)}(l-l') = |\langle \hat{a}^\dagger_l(t)\hat{a}_{l'}(t)\rangle|/\bar{n}$ and normalized correlation $g^{(2)}(l-l')$ that spatially oscillate with the period $d^* = 2\pi/q^*$ (in dimensionless lattice units). These oscillations are spatially attenuated through the presence of a Gaussian envelope whose characteristic scale $\Delta(t)$, given by Eq. (8), grows as $\sim t^{1/2}$ with time. A crystal-like order therefore first emerges locally in this driven lattice, between adjacent lattice sites, and then spreads out over the entire condensate wavefunction, in a diffusion-like process, potentially up to the entire sample size, until the matter-wave coherence is ultimately destroyed due to secondary atom-atom collision processes.

This spreading is also found in the Truncated-Wigner modelling (see section 4), and is illustrated in Fig. S2, showing normalized correlations that are numerically computed for the parameter set $s_0 = 3.4$, $\nu = 30$ kHz, $\varphi_0 = 20^o$, $N = 10^5$, $\omega_x = 2\pi \times 20$ Hz, and $\omega_y = \omega_z = 2\pi \times 30$ Hz, at various evolution times. A comparison with the corresponding momentum distribution as a function of time, Fig. S2**(e)**, shows that this diffusion process across the condensate wavefunction is accomplished at the time scale when the side-peak substructure in the time-of-flight images become fully visible.

A key parameter for a maximally rapid spreading of these oscillations across the lattice is therefore the effective diffusion constant describing this spreading process, which is proportional to the sharpness of the instability peak described by the second derivative λ''. It is thus the existence of sharp features in the coupled-band system that allows for an extended order to appear in the system. Within the tight-binding model, these sharp features are enhanced by the slope of the crossing band (J_1), and decrease for an increasing coupling element W, which broadens the avoided crossings in the spectrum. In the parameter range considered here, an increasing interaction parameter nU increases both the maximum instability exponent λ_* and the second derivative λ''. While the decay scale $\Delta(t) \propto t^{1/2}$ can, in principle, also be enhanced by increasing the evolution time t, letting the system evolve for too long a time leads to a breakdown of the Bogolubov approximation, entailing secondary atom-atom scattering processes and a global loss of coherence.

3. Estimation of the interaction parameter

The interaction parameter nU in the effective 1D model has to take into account the fact that the real system is a 1D lattice of pancakes of atoms. In order to account for weakly populated sites, where the interaction can be described perturbatively, and strongly populated sites, with a transverse Thomas-Fermi profile, we use a heuristic interpolation formula [3, 4] for the interaction energy U on site ℓ:

$$U_\ell = \frac{2\hbar\omega_\perp a_s/(\sqrt{2\pi}a_0)}{\sqrt{1+4n_\ell a_s/(\sqrt{2\pi}a_0)}}, \tag{11}$$

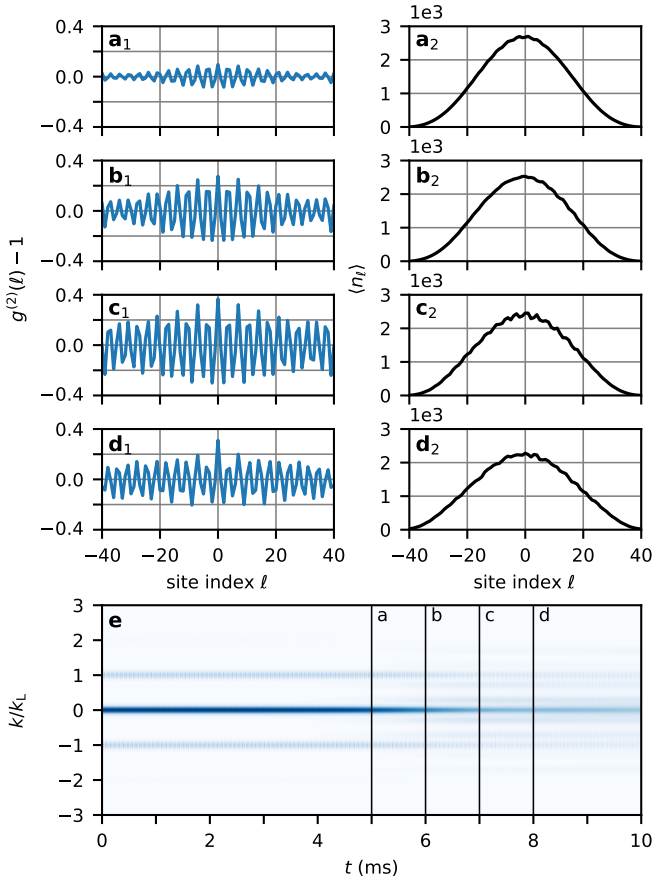

FIG. S2. Diffusive spreading of correlations across the lattice, calculated for $s_0 = 3.4$, $\nu = 30$ kHz, $\varphi_0 = 20^\circ$, $N = 10^5$, with hybrid trap parameters $\omega_x = 2\pi \times 20$ Hz and $\omega_y = \omega_z = 2\pi \times 30$ Hz. Simulation results are shown at times **($\mathbf{a_1}$,$\mathbf{a_2}$)** $t = 5$ ms, **($\mathbf{b_1}$,$\mathbf{b_2}$)** $t = 6$ ms, **($\mathbf{c_1}$,$\mathbf{c_2}$)** $t = 7$ ms, **($\mathbf{d_1}$,$\mathbf{d_2}$)** $t = 8$ ms. First column: density-density correlations $g^{(2)}(l)$ between the lattice sites l and $l' = 0$ in the lowest band, The second column shows the corresponding mean lattice site populations. While at $t = 5$ ms the oscillations in the density-density correlations are decaying on a scale of about 20 lattice sites, they cover the entire atomic sample with minimal decay at $t = 7$ ms. **(e)** For the same parameter set, numerically simulated momentum distribution of the atoms as a function of the evolution time. Note that the appearance of the side peaks in the momentum distribution coincides with the time scale $t \sim 7$ ms at which the correlations spread over the whole condensate (c_1,c_2).

where n_ℓ is the number of atoms on site ℓ, $\omega_\perp$ is the geometrical average transverse frequency ($\omega_\perp/(2\pi) = 67$ Hz), a_s is the scattering length of ^{87}Rb ($a_s \simeq 5.3$ nm), and a_0 is the characteristic size of the ground state of the lattice potential well in the harmonic approximation: $a_0 = \sqrt{\hbar^2/(mE_L\sqrt{s})} = ds^{-1/4}/(\pi\sqrt{2}) \simeq 86$ nm.

Within this approximation, we can estimate the maximum value of the interaction parameter nU. Taking an initial Thomas-Fermi profile for the BEC in the dipole trap with frequencies $(\omega_{x'}, \omega_{y'}, \omega_z) = 2\pi \times (10.4, 66, 68)$ Hz, and a total number of atoms $N = 5 \times 10^5$, we estimate that the number of atoms loaded in the central site of the lattice ($\ell = 0$) is $n_0 \simeq 4.4 \times 10^3$. We can then compute the maximum value n_0U_0/E_L:

$$\frac{n_0U_0}{E_L} \simeq \frac{\hbar\omega_\perp}{E_L}\sqrt{\frac{a_s}{\sqrt{2\pi}a_0}}\sqrt{n_0} \simeq 0.086. \tag{12}$$

This justifies our choice of the range of values for nU in the tight-binding model (Section 2).

4. Numerical simulations : truncated Wigner

Numerical simulations were performed using the Truncated Wigner method [5–7] which allows one to account for the effect of quantum fluctuations. This method was implemented on the basis of a multiband description of the lattice problem at hand, using the Wannier orbitals $\chi_{n,\ell}(x) = \chi_{n,0}(x - \ell d)$ that are obtained from the inverse Fourier transform of the Bloch eigenstates of the homogeneous one-dimensional lattice described by the Hamiltonian:

$$H_0 = \frac{\hat{p}^2}{2m} - \frac{s_0}{2}E_L\cos(k_Lx) \tag{13}$$

with $\hat{p} = -i\hbar\partial/\partial x$. Here, $\ell \in \mathbb{Z}$ is the lattice site index and n represents the band index ranging between 0, corresponding to the ground band, and a maximum excitation number M chosen such that all relevant driving-induced intrawell coupling processes are accounted for in this representation. The Wannier orbitals are mutually orthogonal and normalized,

$$\int_{-\infty}^{\infty}\chi^*_{n,\ell}(x)\chi_{n',\ell'}(x)dx = \delta_{nn'}\delta_{\ell\ell'}\,, \tag{14}$$

and fulfill the parity property

$$\chi_{n,0}(-x) = (-1)^n\chi_{n,0}(x) \tag{15}$$

owing to the symmetry of the lattice wells. On-site energies E_n and nearest-neighbor hoppings J_n associated with the n^{th} excited band are calculated from the relations

$$\int_{-\infty}^{\infty}\chi^*_{n,\ell}(x)H_0\chi_{n',\ell}(x)dx = E_n\delta_{nn'}\,, \tag{16}$$

$$\int_{-\infty}^{\infty}\chi^*_{n,\ell}(x)H_0\chi_{n',\ell\pm1}(x)dx = -J_n\delta_{nn'}\,, \tag{17}$$

respectively, while tunneling matrix elements beyond the nearest neighbors are neglected in the description.

We also neglect interaction effects involving Wannier orbitals on different sites, thus only accounting for on-site interaction matrix elements obtained from the integrals

$$u_{n_1n_2n'_1n'_2} = \int_{-\infty}^{\infty}\chi^*_{n_1,\ell}(x)\chi^*_{n_2,\ell}(x)\chi_{n'_1,\ell}(x)\chi_{n'_2,\ell}(x)dx \tag{18}$$

which, owing to the property (15), vanish if $n_1 + n_2 + n_1' + n_2'$ is an odd number. Lattice shaking is incorporated through the gauge transformation

$$\psi \mapsto \tilde{\psi} = \exp\left[-\frac{i\varphi_0}{\hbar k_\mathrm{L}}\cos(2\pi\nu t)\hat{p}\right]\psi \tag{19}$$

of the wavefunction, which effectively yields a periodically modulated synthetic gauge field. The associated matrix elements in the Wannier basis are given by

$$p_{nn'}^{(\ell-\ell')} = \int_{-\infty}^{\infty} \chi_{n,\ell}^*(x)\hat{p}\chi_{n',\ell'}(x) \tag{20}$$

and vanish for $\ell = \ell'$ if $n + n'$ is an even number.

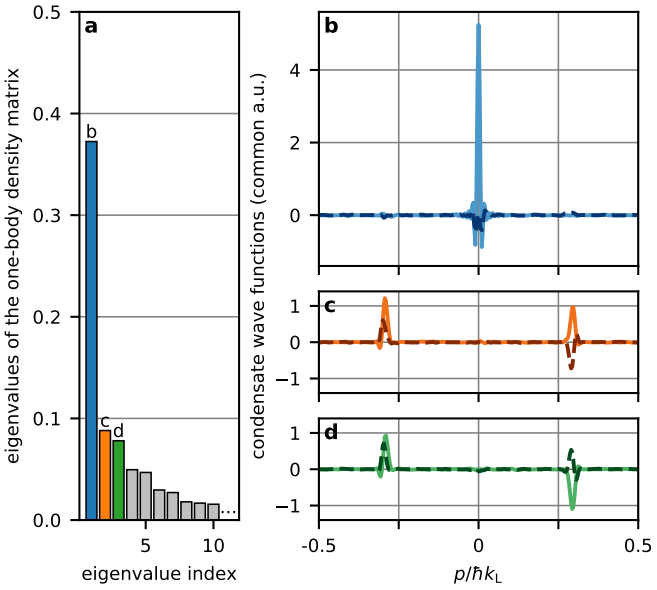

FIG. S3. **(a)** Eigenvalues of the reduced one-body density matrix, normalized with respect to the total population of the atomic gas. Three eigenvalues are distinctly large with respect to the others, indicating the presence of Bose-Einstein condensates. **(b-d)** Ground-band components of the corresponding three associated condensate wavefunctions (obtained via the eigenvectors of the reduced one-body density matrix multiplied by the square roots of the associated eigenvalues) plotted in momentum space (solid line: real part; dashed line: imaginary part of the ground-mode wavefunction), in matching colors. Besides the primary condensate centered about $p = 0$, two secondary condensates, corresponding to linear combinations of left- and right-moving states $e^{\pm iq^*x}$, are populated through four-wave mixing. Parameters: $s_0 = 3.4$, $\nu = 30$ kHz, $\varphi_0 = 20^\mathrm{o}$, $N = 10^5$, $t = 5$ ms.

Neglecting driving-induced couplings beyond nearest neighbors, we obtain the time evolution equations for the calculations of trajectories in the framework of the quasi-classical Truncated Wigner method as

$$\begin{aligned} i\hbar\frac{\partial}{\partial t}\psi_{n,\ell}(t) = {} & (E_n + V_\ell)\psi_{n,\ell}(t) - J_n[\psi_{n,\ell+1}(t) + \psi_{n,\ell-1}(t)] \\ & -\varphi_0\frac{2\pi\nu}{k_\mathrm{L}}\sin(2\pi\nu t)\sum_{n'=0}^{M}\sum_{\ell'=\ell-1}^{\ell+1} p_{nn'}^{(\ell-\ell')}\psi_{n',\ell'}(t) \\ & +g_\ell\sum_{n',n_2,n_2'=0}^{M} u_{nn_2n'n_2'}\psi_{n_2,\ell}^*(t)\psi_{n_2',\ell}(t)\psi_{n',\ell}(t) \\ & -g_\ell\sum_{n',n_2=0}^{M} u_{nn_2n'n_2}\psi_{n',\ell}(t) \end{aligned} \tag{21}$$

with

$$V_\ell = \frac{1}{2}m\omega_x^2 d^2\ell^2 \tag{22}$$

the shift of the on-site energies due to the longitudinal confinement of the hybrid trap and

$$g_\ell = (\sqrt{2\pi}/a_0)U_\ell = \frac{2\hbar\omega_\perp a_\mathrm{s}}{\sqrt{1 + 4n_\ell a_\mathrm{s}/(\sqrt{2\pi}/a_0)}} \tag{23}$$

the effective on-site interaction parameter modified by the presence of the transverse confinement, as described in Sec. 3. The lattice site populations n_ℓ are numerically obtained from imaginary-time propagation yielding the initial condensate wavefunction in the un-driven lattice, and we assume here that they vary only marginally in the course of time evolution (which is not always the case, as seen in Fig. 4). Note that the last term in Eq. (21) arises from the proper derivation of the classical counterpart of the quantum interaction term via Weyl ordering.

The Truncated Wigner method allows one to compute quasi-classical expressions for the mean populations $\langle\hat{n}_{n,\ell}\rangle$ of the lattice sites as well as for the population correlations $\langle\hat{n}_{n,\ell}\hat{n}_{n',\ell'}\rangle$, where Weyl ordering has to be respected in order to correctly obtain the quantum expectation values from the classically calculated densities $|\psi_{n,l}(t)|^2$. It can also give access to the entire reduced one-body density matrix constituted by the expectation values of the coherence matrix elements $\langle\hat{a}_{n,\ell}^\dagger\hat{a}_{n',\ell'}\rangle$ (see Ref. [8] for a similar study). Diagonalization of this matrix yields the proper definition of the condensate fraction, via the eigenvector that is associated with its largest eigenvalue [9]. We can thereby monitor the time evolution of the shape and population of the condensate, and the appearance and ultimate destruction of the non-commensurate crystal-like order.

Within the time window where the emerging periodic order is realized, the formation of two secondary Bose-Einstein condensates can be identified in the eigenspectrum of the reduced one-body density matrix, namely via the presence of two further eigenvalues that are distinctly large as compared to the rest of the spectrum. As displayed in Fig. S3, those two secondary condensate wavefunctions correspond to linear combinations of

the two traveling waves $e^{\pm iq^*x}$ that are populated via four-wave-mixing. The superposition of those secondary condensates with the primary condensate centered about $p = 0$ in momentum space gives rise to the coherence oscillations displayed in Fig. 4.

5. Experimental method : band-mapping

To more accurately identify the onset of the emerging periodic order, we use the band-mapping technique [10] that consists in decreasing adiabatically the lattice before the time-of-flight (see Fig. S4). The band-mapping reveals the hybrid nature of the unstable modes induced by resonant coupling. The clear growth of the population fraction in the higher coupled band is subsequently plotted as a function of time to characterize the kinetics of the crystal-like state formation and its persistence over time (see Fig. S5).

[1] Y.-J. Lin, A. R. Perry, R. L. Compton, I. B. Spielman, and J. V. Porto, Rapid production of ^{87}Rb bose-einstein condensates in a combined magnetic and optical potential, Phys. Rev. A **79**, 063631 (2009).

[2] Y. Castin and R. Dum, Low-temperature Bose-Einstein condensates in time-dependent traps: Beyond the u(1) symmetry-breaking approach, Phys. Rev. A **57**, 3008 (1998).

[3] T. Paul, M. Hartung, K. Richter, and P. Schlagheck, Nonlinear transport of Bose-Einstein condensates through mesoscopic waveguides, Phys. Rev. A **76**, 063605 (2007).

[4] E. Michon, C. Cabrera-Gutiérrez, A. Fortun, M. Berger, M. Arnal, V. Brunaud, J. Billy, C. Petitjean, P. Schlagheck, and D. Guéry-Odelin, Phase transition kinetics for a Bose Einstein condensate in a periodically driven band system, New Journal of Physics **20**, 053035 (2018).

[5] M. J. Steel, M. K. Olsen, L. I. Plimak, P. D. Drummond, S. M. Tan, M. J. Collett, D. F. Walls, and R. Graham, Dynamical quantum noise in trapped Bose-Einstein condensates, Phys. Rev. A **58**, 4824 (1998).

[6] A. Sinatra, C. Lobo, and Y. Castin, The truncated Wigner method for Bose-condensed gases: limits of validity and applications, Journal of Physics B: Atomic, Molecular and Optical Physics **35**, 3599 (2002).

[7] A. Polkovnikov, Phase space representation of quantum dynamics, Annals of Physics **325**, 1790 (2010).

[8] R. Wanzenböck, S. Donsa, H. Hofstätter, O. Koch, P. Schlagheck, and I. Březinová, Chaos-induced loss of coherence of a Bose-Einstein condensate, Phys. Rev. A **103**, 023336 (2021).

[9] O. Penrose and L. Onsager, Bose-Einstein Condensation and Liquid Helium, Phys. Rev. **104**, 576 (1956).

[10] M. Greiner, I. Bloch, O. Mandel, T. W. Hänsch, and T. Esslinger, Exploring Phase Coherence in a 2D Lattice of Bose-Einstein Condensates, Phys. Rev. Lett. **87**, 160405 (2001).

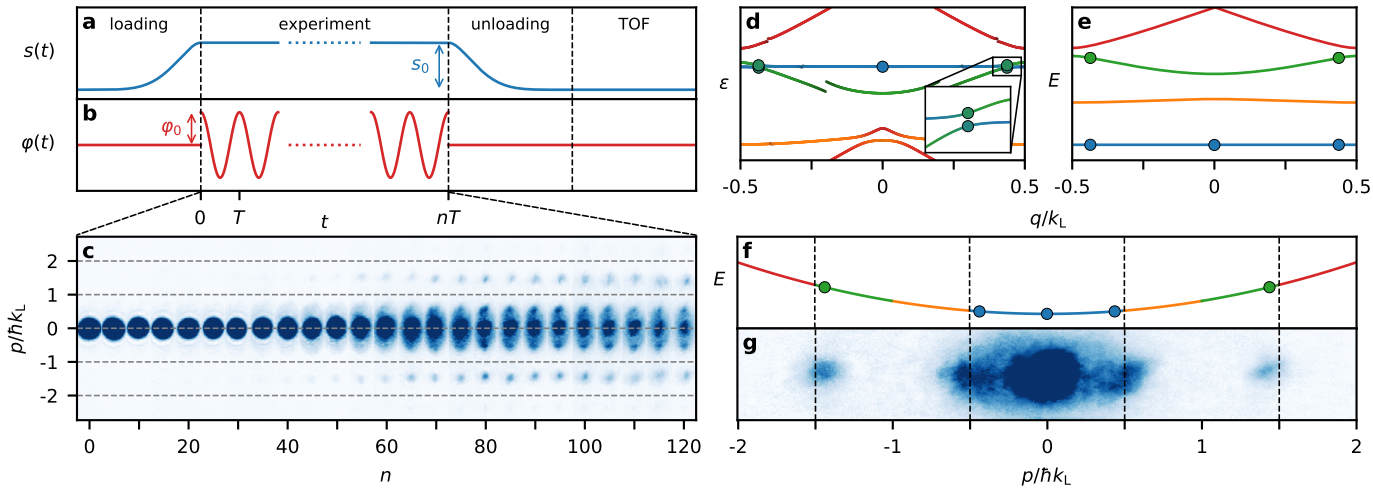

FIG. S4. **Band-mapping process.** **(a)** Depth of the lattice along time: adiabatical loading at s_0, held constant during the experiment, adiabatical unloading to band map (see text) and switch off for time-of-flight imaging. **(b)** Phase of the lattice along time, sine-modulated with amplitude φ_0 for an integer number n of periods T. **(c)** Stack of experimental absorption images for increasing n, with $s_0 = 3.70 \pm 0.10$, $\varphi_0 = 15^\circ$, $\nu = 1/T = 25.5$ kHz and $t_{\mathrm{TOF}} = 35$ ms. **(d)** Corresponding quasi-energy spectrum (colored lines) where the overlaps between the Floquet eigenstates and the eigenstates of the static lattice have been color-coded, with blue, orange, green and red corresponding respectively to the first 4 bands (s to f). BEC (disk in $q = 0$) and instability (disks in $q \neq 0$) modes. **(e-f)** Band structures of the lattices of depth $s_0 = 3.7$ for (e) and $s_0 = 0$ for (f) (solid colored lines) and follow-up of the modes (see text) with the same color code. **(f-g)** BZ borders (black dotted lines). **(g)** Absorption image after $n = 80$ periods of data (c).

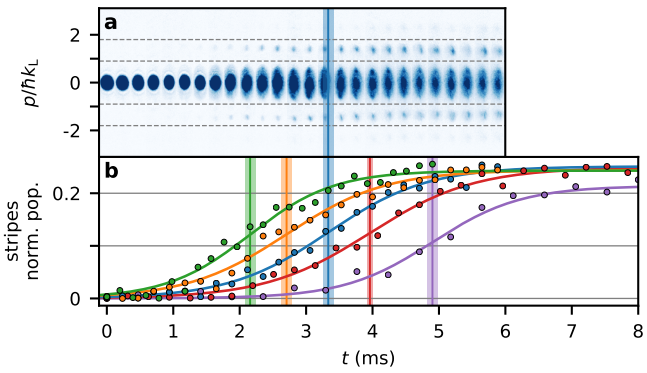

FIG. S5. **Timescales measurements.** **(a)** Example of measured data series after band-mapping, for $s_0 = 3.70 \pm 0.20$, $\nu = 25.5\,\mathrm{kHz}$ and $\varphi_0 = 15^\circ$. The population from higher bands in the horizontal grey shaded stripes is measured over time to extract a nucleation time. **(b)** Growth curves extracted as in **(a)** for the points of Fig. 4(b) corresponding to coupling bands s and d, with the purple, red, blue, orange, and green data corresponding to $\varphi_0 = \{10^\circ, 12.5^\circ, 15^\circ, 17.5^\circ, 20^\circ\}$ respectively. The sigmoid fitting curves are shown and the extracted nucleation times are represented by vertical lines, with shaded areas denoting the uncertainty from the fit.